

# Development of lunar regolith-based composite for *in-situ* 3D printing via high-pressure extrusion system

Hua ZHAO<sup>a</sup>, Jihong ZHU (✉)<sup>a,b</sup>, Shangqin YUAN (✉)<sup>a,c</sup>, Shaoying LI<sup>a</sup>, Weihong ZHANG<sup>a</sup>

<sup>a</sup> State IJR Center of Aerospace Design and Additive Manufacturing, School of Mechanical Engineering, Northwestern Polytechnical University, Xi'an 710072, China

<sup>b</sup> Key Laboratory of Metal High Performance Additive Manufacturing and Innovative Design, MIIT China, Northwestern Polytechnical University, Xi'an 710072, China

<sup>c</sup> Unmanned System Research Institute, Northwestern Polytechnical University, Xi'an 710072, China

✉ Corresponding author. E-mails: [jh.zhu@nwpu.edu.cn](mailto:jh.zhu@nwpu.edu.cn) (Jihong ZHU); [shangqin.yuan@nwpu.edu.cn](mailto:shangqin.yuan@nwpu.edu.cn) (Shangqin YUAN)

© Higher Education Press 2023

**ABSTRACT** To fully utilize the *in-situ* resources on the moon to facilitate the establishment of a lunar habitat is significant to realize the long-term residence of mankind on the moon and the deep space exploration in the future. Thus, intensive research works have been conducted to develop types of 3D printing approach to adapt to the extreme environment and utilize the lunar regolith for *in-situ* construction. However, the *in-situ* 3D printing using raw lunar regolith consumes extremely high energy and time. In this work, we proposed a cost-effective melting extrusion system for lunar regolith-based composite printing, and engineering thermoplastic powders are employed as a bonding agent for lunar regolith composite. The high-performance nylon and lunar regolith are uniformly pre-mixed in powder form with different weight fractions. The high-pressure extrusion system is helpful to enhance the interface affinity of polymer binders with lunar regolith as well as maximize the loading ratio of *in-situ* resources of lunar regolith. Mechanical properties such as tensile strength, elastic modulus, and Poisson's ratio of the printed specimens were evaluated systematically. Especially, the impact performance was emphasized to improve the resistance of the meteorite impact on the moon. The maximum tensile strength and impact toughness reach 36.2 MPa and 5.15 kJ/m<sup>2</sup>, respectively. High-pressure melt extrusion for lunar regolith composite can increase the effective loading fraction up to 80 wt.% and relatively easily adapt to extreme conditions for *in-situ* manufacturing.

**KEYWORDS** *in-situ* resource utilization, melt extrusion molding, lunar regolith-based composites, mechanical properties, additive manufacturing

## 1 Introduction

The rapid development of space technology has prompted mankind to gradually get rid of the shackles of the earth and begin to explore deep space [1]. The lunar exploration has always been the central benefit of space competition due to the special geographic location and abundant natural resources on the moon [2–4]. Since the United States successfully completed the manned moon landings in the 1960s and 1970s, how to establish an extraterrestrial habitat on the moon to facilitate the long-term residence of mankind has become a hot research topic [5,6]. The construction of the lunar habitat not only needs to protect mankind from the terrible environment of

the moon, such as large temperature differences, high vacuum, meteorite impact, and radiation but also make use of the resources available on the moon as much as possible. This is because transportation of construction materials from the earth to the moon is economically unaffordable. Therefore, many researchers have proposed the lunar *in-situ* resource utilization (ISRU) technology [7–10], which utilizes the abundant lunar regolith resources on the moon to produce architectural and functional structures.

The lunar regolith materials are widely distributed on the surface of the moon and can be conveniently obtained in large quantities [11,12]. In addition, the lunar regolith is an ideal material for the construction of lunar habitat due to its excellent environmental suitability in terms of thermal and radiation protection [13]. A large number of

scholars have conducted detailed studies on the abundant lunar regolith samples brought back from the moon by the Apollo program of the United States. Meanwhile, Chinese scholars have also studied the chemical composition and physical properties of the lunar regolith brought back by the Chang'e-5 probe, and have achieved very significant results [14–18]. The results show that the chemical composition and physical properties of the lunar regolith material are very similar to that of the basalt produced by the volcanic eruptions on the earth [19,20]. To continuously investigate how to complete the lunar habitat construction with lunar regolith, a variety of lunar regolith simulants [21–23] (such as JSC-1, JSC-1A, and CAS-1) have been developed by utilizing the basalt from volcanic eruptions, which strive to be consistent with the actual lunar regolith in terms of chemical composition, particle size distribution, shear resistance, complex permittivity, and reflectance spectra.

Dozens of researches on the utilization of lunar regolith for lunar habitat construction have been published [24,25]. The lunar regolith cement is synthesized by adding sulfur or alkaline activator to the lunar regolith and then processed into cylindrical and block structures by casting or extrusion to study the mechanical properties [26–30]. Compared with the traditional methods of lunar regolith-based cement development, additive manufacturing (AM) technology provides a very novel way to build the lunar habitat because of its rapid prototyping and almost no restrictions on structural geometry. Cesaretti et al. [31] developed a particular patented 3D printing process D-shape, which sprayed adhesive on each layer of lunar regolith to complete the construction of the lunar habitat model. Krishna Balla et al. [32] utilized the laser-engineered net shaping technology developed by Sandia National Laboratory of the United States to manufacture the lunar regolith components, which preliminarily proved the feasibility of this process for lunar regolith 3D printing. Zhao et al. [33] developed a laser-assisted sintering process to fabricate the lunar regolith composites and then established the relationship between process parameters and mechanical properties. Meurisse et al. [34] demonstrated the feasibility of solely utilizing the concentrated sunlight to sinter the lunar regolith layer-by-layer, while the quality of sintering was difficult to meet the demand for lunar habitat construction. Goulas et al. [35–37] and Fateri and Gebhardt [38] fabricated some block samples with lunar regolith on the preheated stainless steel substrate plates by selective laser melting technology, which exhibited high hardness but poor performance in porosity. In addition, Liu et al. [39] produced the architectural and functional structures with the mixed slurry of lunar regolith powders and photosensitive resin using digital light processing technology and then were sintered in a sintering furnace to complete the final structure. The printed structures have excellent mechanical properties and prototyping

accuracy. However, the process is complicated, and the photosensitive resin material will be wasted during the sintering process, which conflicts with the concept of ISRU on the moon.

Although the aforementioned research initially proved the feasibility of using lunar regolith for 3D printing, it confronted the difficulty of matching the complexity of AM process with the quality of the printed structure. Melted extrusion molding technology using lunar regolith-based composite has become an alternative AM strategy for lunar regolith *in-situ* manufacturing and lunar habitat construction due to that it is relatively convenient, cost-effective, environmentally tolerable, and wide range of candidate materials. Jakus et al. [40] fabricated a robust and elastic structure utilizing direct extrusion process with the inks synthesized by simple mixing of the lunar regolith simulant JSC-1A, polylactic-co-glycolic acid, and organic solvents, while a variety of auxiliary materials increase the cost and complexity. Therefore, in order to fully improve the ISRU, it is necessary to maximize the use of lunar regolith and reduce the complexity of 3D printing process.

In this work, the lunar regolith-based composite is developed for melt extrusion molding to evaluate the process feasibility and printed material performance for future ISRU on the moon. The melt extrusion molding presented in this work is to directly extrude the molten lunar regolith-based composite materials, which has a simple equipment structure and high process stability compared to the laser sintering molding process. In addition, the pellets or powders can be used directly as raw materials, which can adapt to different shapes and sizes of lunar regolith materials. Meanwhile, the extrusion screw can ensure the mixing uniformity of the lunar regolith-based composites and improve the performance of the printed structures, which is very suitable for future lunar surface construction fabrication. The lunar regolith-based composite powders consist of lunar regolith simulants of basalt and nylon powders with different weight fractions. The thermal property, morphology, and flow capability of pre-mixed composite powders are evaluated to quantify the powder properties and determine the process window. A full factorial design of experimental was carried out to study the influence of weight fractions, printing speed, and printing temperature on the tensile mechanical properties of melt extrusion printed specimens. Meanwhile, excellent impact resistance is achieved at the basalt weight fraction of 60 wt.%. Finally, the developed composite feedstocks are utilized for the robot-assisted high-pressure melt extrusion 3D printing system for large component fabrication. The lunar habitat architectural model has been printed with lunar regolith composite to evaluate the feasibility of melt extrusion technology for lunar *in-situ* manufacturing.

## 2 Experimental

### 2.1 Materials

The material composition of the lunar regolith is mainly oxides, especially the silicas account for the largest ratio, which is basically analogous to the composition of basalt materials on the earth [41]. Table 1 shows the material composition of the lunar regolith collected by Apollo 14, CE-5, and the basalt in different regions on the earth. The basalt used in this study was purchased from Deze Mineral Products Co., Ltd., and laser particle size analysis was performed on the basalt size distribution. As shown in Fig. 1, the particle size of basalt is mainly distributed between 50 and 200  $\mu\text{m}$ , and the volume ratio reaches 78.5%. The mean particle size and median particle size of basalt powder are 101.084 and 97.923  $\mu\text{m}$ , respectively, which are within the mean and median particle sizes of the lunar regolith material at the Apollo 11–17 landing sites [21]. Therefore, it is reasonable to use the basalt as the lunar regolith simulant. The PA12 powder (PA2200, supplied by EOS, Germany) was a commonly used thermoplastic polymer with excellent comprehensive performance. PA12-Basalt composites were prepared by utilizing a magnetic stirrer to uniformly mix PA12 and basalt powders with three different basalt weight fractions of 40, 50, and 60 wt.% (refer to herewith as PA12-Basalt40wt.%, PA12-Basalt50wt.%, and PA12-Basalt-60wt.%).

**Table 1** Weight fraction with material composition of lunar regolith and simulants

Sample	Weight fraction/wt. %								
	SiO <sub>2</sub>	TiO <sub>2</sub>	Al <sub>2</sub> O <sub>3</sub>	FeO	MgO	CaO	Na <sub>2</sub> O	K <sub>2</sub> O	Others
Apollo 14	48.10	1.70	17.40	10.40	9.40	10.70	0.70	0.55	1.05
CE-5	42.20	5.00	10.80	22.50	6.48	11.00	0.26	0.19	1.57
Basalt-1#	54.48	1.39	14.89	8.66	6.31	7.16	2.71	0.39	4.01
Basalt-2#	45.90	4.87	12.17	8.71	9.58	7.82	3.25	1.81	5.89
Basalt-3#	50.02	0.92	15.78	7.60	6.12	8.96	2.85	0.32	7.43

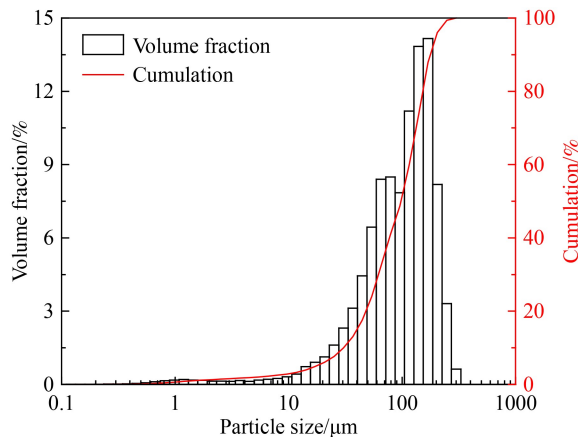


**Fig. 1** Particle size distribution of lunar regolith simulant.

### 2.2 Thermal analysis

#### 2.2.1 Differential scanning calorimetry

Differential scanning calorimetry (DSC) was conducted on a DSC instrument (200 F3, NETZSCH, Germany) to measure the melting and crystallization characteristics of three PA12-Basalt composite powders under nitrogen protection gas with a flow rate of 50 mL/min. Each of the composite powder samples with the weight of 5 mg was put into the aluminum crucible. The heating and cooling process was performed from 25 to 250 °C at a rate of 10 °C/min. Posteriorly to the DSC tests, the melting and crystallization temperature interval of PA12-Basalt composite material, as well as the width of the glass window can be obtained.

#### 2.2.2 Thermogravimetric analysis

Thermogravimetric analysis (TGA) of three samples (PA12-Basalt40wt.%, PA12-Basalt50wt.%, and PA12-Basalt60wt.%) was performed on an STA instrument (STA 449 F3, NETZSCH, Germany) under the argon purge of 60 mL/min. The temperature varied from 35 to 650 °C with a consistent heating rate of 20 °C/min and a natural cooling process.

### 2.3 Microstructure characterization

To obtain satisfactory observation results, three non-conductive PA12-Basalt composite powder samples were sprayed with gold by Ion Sputtering Instrument (MC1000, HITACHI, Japan), and then placed on the sample stage of the scanning electron microscope (SEM, TM 4000 PLUS, HITACHI, Japan) in a vacuum environment. The microscopic morphology of the samples could be observed under the conditions of 15 kV voltage and 200, 500 magnifications. Besides, the micromorphology of three standard printed specimens under different weight fractions (PA12-Basalt40wt.%, PA12-Basalt50wt.%, and PA12-Basalt60wt.%) with the same specific process parameter was characterized by utilizing a digital optical microscope (VHX-6000, Keyence, Japan) to observe the distribution of basalt particles, printing defects, and layer-to-layer bonding.

### 2.4 Specimens fabrication via melt extrusion molding

The schematic diagram of the printer for the lunar regolith composite is shown in Fig. 2, where the piston-based pellet extruder produced by Shanghai Fochif Electromechanical Technology Co., Ltd. was used to print PA12-Basalt composite materials for small-batch material performance experiments, and the screw-based

pellet extruder was used to verify the feasibility of printing large-scale structures. Add the PA12-Basalt composite powder into the heating chamber of the piston-based pellet extruder. After the material is fully melted, the stepper motor drives the piston rod to extrude the molten material from the nozzle and cooperates with the movement of the  $X$ - $Y$ - $Z$  direction stepper motor to complete the 3D printing of the structure.

In this research, the motor-assisted microsyringe (MAM) software developed by the equipment manufacturer was used to set the process parameters and generate G-code. The ASTM D638-14 and GB/T 229-2007 standards were applied for tensile and impact testing, respectively. The geometric parameters of the standard specimens for tensile and impact testing are shown in Fig. 3, where (a) represents the tensile specimen and (b) represents the impact specimen. The computer-aided design model of specimens was completed by using SolidWorks software and exported as an STL model importing to the MAM software.

The process parameters utilized in the production of the tensile specimens are shown in Table 2. The processes of printing temperature and printing speed were selected to investigate the influence of process parameters on the

mechanical properties of printed tensile specimens. As shown in Table 2, all tensile specimens were printed with two external contours around the dog-bone geometry and the infill was printed by alternating  $45^\circ$  and  $-45^\circ$  layers in 100%. The schematic diagrams of the internal infill pattern and path of the dog-bone specimen are shown in Fig. 4, where (a) represents the infill pattern, and (b) represents the  $45^\circ$ - $-45^\circ$  rectilinear infill path.

The process parameters utilized in the production of the impact specimens are shown in Table 3. All impact specimens were printed at a given printing temperature and printing speed. As well, to study the influence of the internal infill angle of the impact specimens on the impact mechanical properties, two alternating infill paths of  $45^\circ$ - $-45^\circ$  and  $0^\circ$ - $90^\circ$  were selected for comparison. The schematic diagram of the internal infill path of the V-shaped impact specimen is shown in Fig. 5, where (a) represents the  $45^\circ$ - $-45^\circ$  infill path, and (b) represents the  $0^\circ$ - $90^\circ$  infill path.

## 2.5 Mechanical testing

Each set of samples consisted of five specimens for a

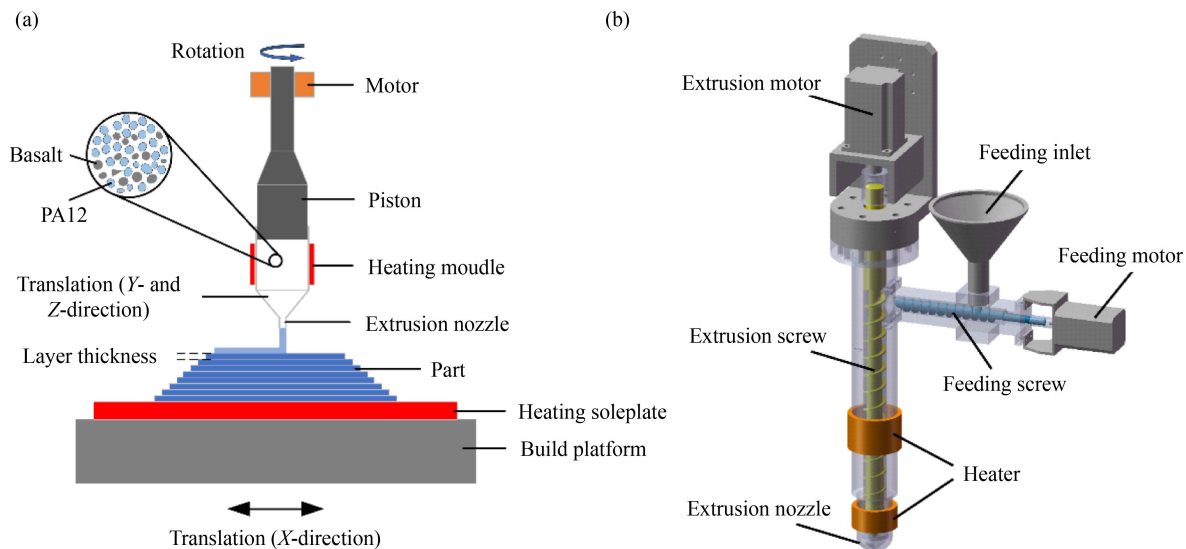


**Fig. 2** Schematic diagram of the printer for the lunar regolith composite: (a) piston-based pellet extruder and (b) screw-based pellet extruder.

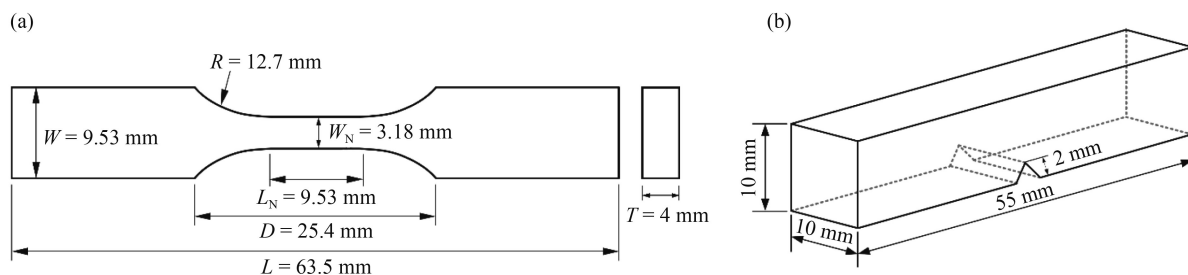


**Fig. 3** Geometric parameters of the standard specimens for mechanical testing: (a) tensile specimen and (b) impact specimen.

given group of process parameters, with a total of 165 specimens (tensile and impact specimens). Due to the physical properties of thermoplastic can vary depending on the ambient environment (especially the temperature and humidity), all of the printed specimens will be preserved in a sealed bag at room temperature for subsequent mechanical properties testing.

The uniaxial tensile testing was carried out according to the standard of ASTM D638-14. To eliminate the influence of ambient temperature on the mechanical properties, the testing was performed at room temperature. A CMT5105 universal electromechanical tensile testing machine manufactured by Shenzhen SENS Testing Instrument Co., Ltd. was used to perform tensile testing with a load cell of 10 kN and a fixed load rate of 2 mm/min. Besides, simultaneously utilizing the PMLAB DIC-3D system can process experimental data to determine the tensile strength  $\sigma_b$  and Young's modulus  $E$ .

The impact testing was performed following the standard of GB/T 229-1994 and utilized the simply

supported beam lateral impact method. The testing was completed by the PIT501J pendulum impact tester produced by Shenzhen Wance Test Equipment Co., Ltd. According to the principle of energy conservation, the impact energy  $A_k$  consumed by breaking the specimen was equal to the potential energy difference before and after the pendulum testing. Hence, the impact toughness  $a_k$  of the specimen can be calculated by the ratio of the impact energy to the area of the fractured section.

### 3 Results and discussion

#### 3.1 Thermal analysis

The physical phase transition process parameters of the lunar regolith composite powders with three different weight fractions during melting and recrystallization are illustrated in Fig. 6. With the increase of the basalt weight fraction, the peak of heat flow during the melting

**Table 2** Process parameters for tensile specimen fabrication

Parameters	Values
Nozzle diameter	1.0 mm
Layer height	0.8 mm
Piston diameter	18 mm
Printing temperature	225, 230, 235 °C
Bed temperature	70 °C
Printing speed	7, 8, 9 mm/s
Extrusion speed	0.02 mm/s
Number of contours	2
Infill percentage	100%
Infill pattern	Rectilinear 45°/-45°

**Table 3** Process parameters for impact specimen fabrication

Parameters	Values
Nozzle diameter	1.0 mm
Layer height	0.8 mm
Piston diameter	18 mm
Printing temperature	230 °C
Bed temperature	70 °C
Printing speed	7 mm/s
Extrusion speed	0.02 mm/s
Number of contours	2
Infill percentage	100%
Infill pattern	45°/-45°, 0°/90°

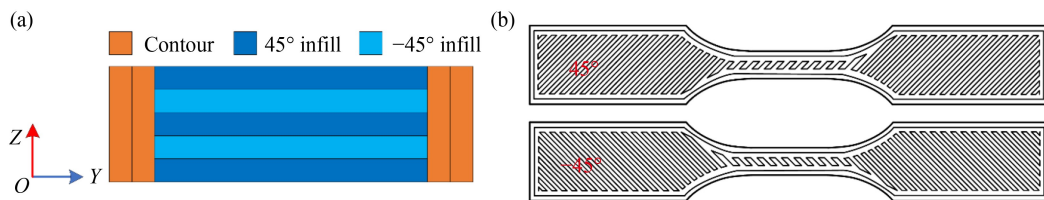


**Fig. 4** Schematic diagram of the internal infill pattern and path for the tensile specimen: (a) infill pattern and (b) 45°/-45° rectilinear infill path.

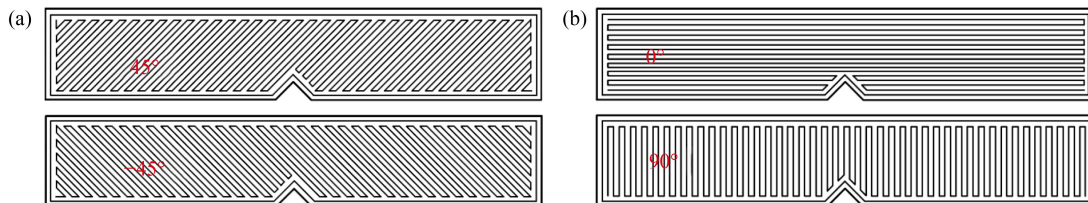


**Fig. 5** Schematic diagram of the internal infill path for the impact specimen: (a) 45°/-45° rectilinear infill path and (b) 0°/90° rectilinear infill path.

endothermic and recrystallization exothermic will decrease, which can be explained by the relative decrease of PA12 content in the phase transition process of melting and recrystallization. Meanwhile, the melting peak temperatures  $T_m$  of the three lunar regolith composite powder samples are almost identical, while the recrystallization peak temperatures  $T_r$  are slightly different. The detailed phase transition process parameters can be obtained from Table 4. As shown in Table 4, the onset melting temperature and offset melting temperature of the three samples hardly varies with the basalt weight fraction, which indicates that the addition of basalt particles has a limited effect on the melting temperature of PA12. On the contrary, the basalt particles have a more significant effect on the recrystallization of PA12. As the weight fraction of basalt increases, the onset and offset temperatures of PA12 recrystallization increase, indicating that the basalt particles promote the recrystallization of PA12 material, which is beneficial for the melt extrusion molding of lunar regolith composite powder.

The mass loss of the lunar regolith composite powders with three different weight fractions due to material decomposition in the TGA testing is shown in Fig. 7. The mass of the three sample materials begins to decrease steadily after reaching the decomposition temperature.

While all the decomposable materials are completely decomposed, the mass of the sample continues to remain stable, which can indicate that only PA12 in the lunar regolith composite powder is decomposed. The detailed onset and offset temperature of decomposition, as well as the mass loss, are shown in Table 5. In order to ensure the PA12 will not be decomposed, the lunar regolith composite powders should be avoided utilizing in an environment above 350 °C. The mass loss of the three samples is not consistent with the theoretical basalt weight fractions, which is mainly due to two reasons: One is that the decomposed PA12 will remain a part of carbon deposited on the sample, and the other is that both PA12 and basalt are solid particles, so it may be very difficult to mix the two materials into an ideal uniform state like a liquid solution. This phenomenon can be observed more clearly from the micromorphology of the three powder samples in Fig. 8.

### 3.2 Microstructure of the lunar regolith-based composite powder

To understand the micromorphology of the lunar regolith composite powder, three sample materials were observed utilizing an SEM. Figures 8(a)–8(c) represent the

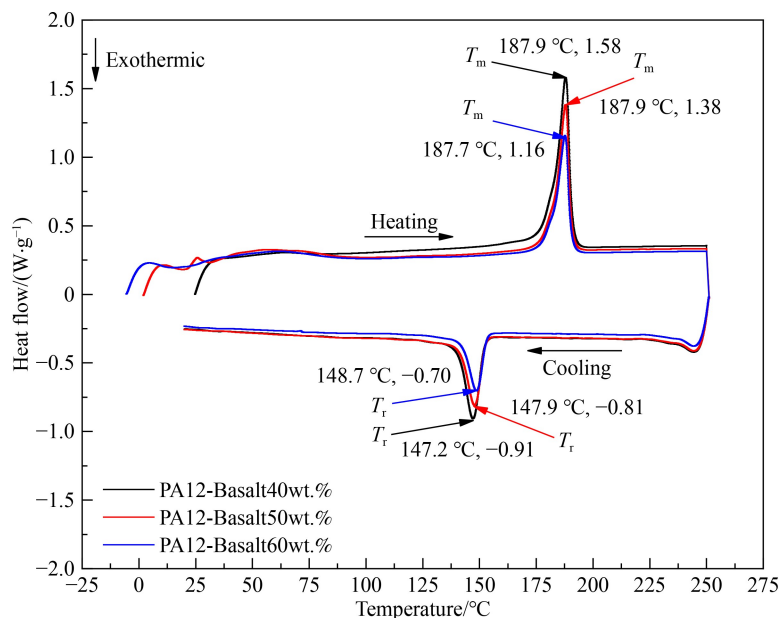


**Fig. 6** Differential scanning calorimetry curves of lunar regolith composite powder at different basalt weight fractions.

**Table 4** Melting and recrystallization properties of PA12-Basalt composite powders

Material	Onset melting temperature/°C	Offset melting temperature/°C	Melting peak/°C	Enthalpy of melting/(J·g <sup>-1</sup> )	Onset recrystallization temperature/°C	Offset recrystallization temperature/°C	Recrystallization peak/°C	Enthalpy of recrystallization/(J·g <sup>-1</sup> )	Glass window width/°C
PA12-Basalt40wt.%	181.6	190.8	187.9	58.03	152.1	140.8	147.2	-31.10	29.5
PA12-Basalt50wt.%	181.6	190.5	187.9	44.54	152.6	141.3	147.9	-26.58	29.0
PA12-Basalt60wt.%	181.5	190.3	187.7	36.03	153.1	142.3	148.7	-21.81	28.4

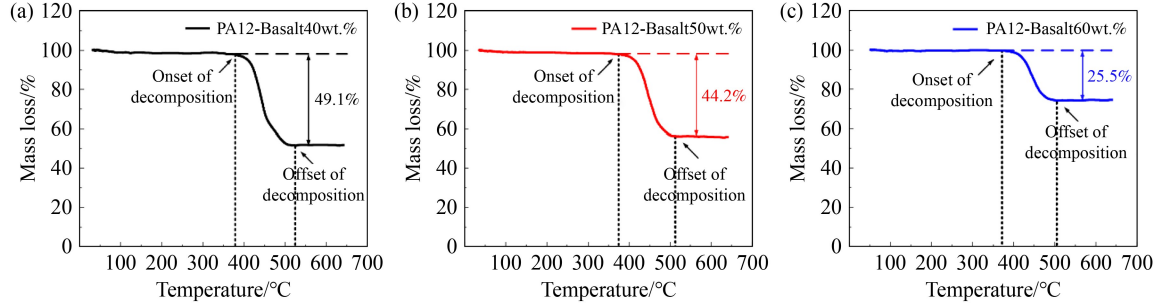


**Fig. 7** Thermogravimetric analysis curves of lunar regolith composite at different basalt weight fractions: (a) PA12-Basalt40wt.%, (b) PA12-Basalt50wt.%, and (c) PA12-Basalt60wt.%.

**Table 5** Decomposition properties of PA12-Basalt composite powders

Material	Onset decomposition temperature/°C	Offset decomposition temperature/°C	Decomposition peak/°C	Mass loss/%
PA12-Basalt40wt.%	375.5	518.6	439.8	49.1
PA12-Basalt50wt.%	372.3	513.2	442.7	44.2
PA12-Basalt60wt.%	371.3	504.4	440.5	25.5

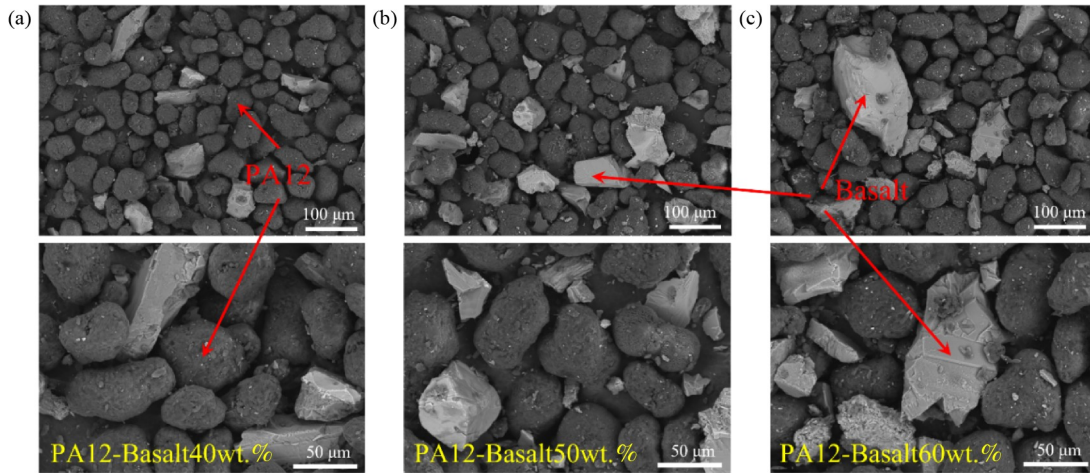


**Fig. 8** Scanning electron microscope images of lunar regolith composite powders: (a) PA12-Basalt40wt.%, (b) PA12-Basalt50wt.%, and (c) PA12-Basalt60wt.%.

micromorphology of the three samples (PA12-Basalt40wt.%, PA12-Basalt50wt.%, and PA12-Basalt60wt.%) under 200 and 500 magnifications, respectively. The darker particles refer to PA12, and the others are basalt. A large amount of PA12 particles is ellipsoid with a relatively regular shape, and the size distribution is also relatively uniform and concentrated, varying from 50 to 90  $\mu\text{m}$ . On the contrary, the basalt particles are of various shapes and the size distribution is relatively dispersed. Under the weathering and erosion of the harsh natural environment of the moon, the lunar regolith almost presents tiny particles of various shapes and sizes. The basalt particles selected in this paper can be used to simulate the lunar regolith material in the natural environment of the moon as realistically as possible. To ensure the mechanical properties of the printed specimens, PA12 and basalt particles demand to

be uniformly mixed. However, due to the differences in micromorphology and mass between PA12 and basalt particles, it is difficult to be completely uniform mixing like a solution.

### 3.3 Mechanical properties

The establishment of a lunar habitat on the moon should not only maximize the use of the *in-situ* resources of the moon but also consider the issues of construction efficiency and energy consumption. Hence, the parameters of lunar regolith simulant weight fraction, printing speed, and printing temperature, which are related to lunar regolith resource utilization, printing efficiency, and energy consumption, respectively, were selected to study the tensile mechanical properties of melt

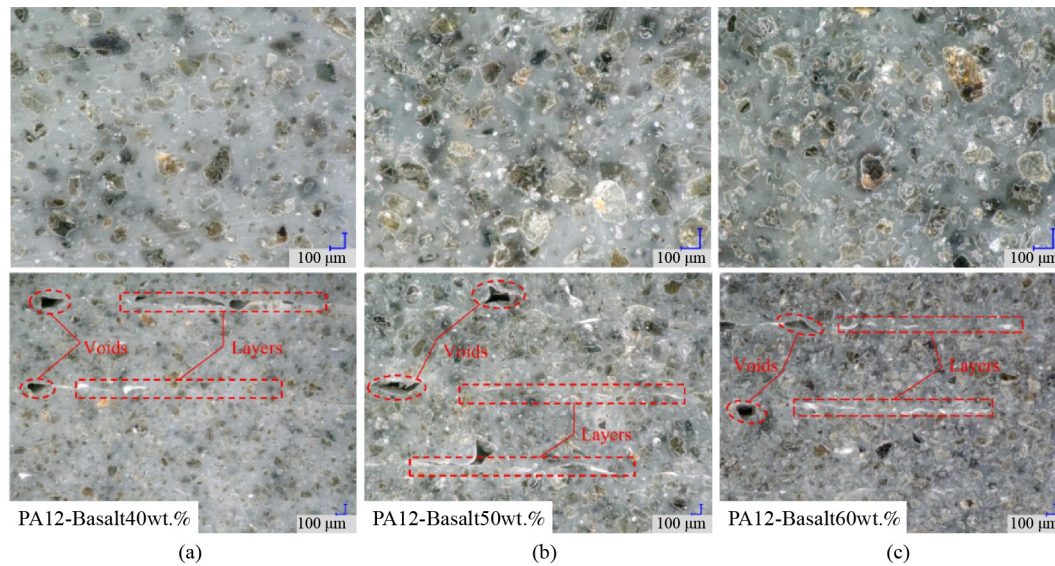


**Fig. 9** Horizontal and tangential micromorphology of printed specimens: (a) PA12-Basalt40wt.%, (b) PA12-Basalt50wt.%, and (c) PA12-Basalt60wt.%.

extrusion printed specimens by a full factorial design of experiments. The weight fraction, printing speed, and printing temperature are all related to the viscosity of the molten lunar regolith-based composite. High viscosity will make the molten material difficult to extrude or reduce the printing speed, thus affecting the printing efficiency. As the weight fraction increases, the viscosity of the molten material will also increase, while an increase in printing temperature will reduce the viscosity of the molten material. Therefore, the process windows of weight fraction, printing speed, and printing temperature need to be obtained by selecting the appropriate viscosity of the molten material. The experimental results are shown in Table 6. The printed specimens of lunar regolith composite with 60 wt.% can be accomplished by the piston-based pellet extruder, and the tensile strength and elastic modulus of the printed specimens have more excellent performance compared with other research works. The weight fraction of the lunar regolith simulant has a more significant effect on the mechanical properties, while the effects of printing speed and printing temperature tend to diminish.

### 3.3.1 Effects of weight fraction on tensile mechanical properties

To reduce the cost of lunar habitat fabrication, it is necessary to maximize the utilization of lunar *in-situ* resources. Figure 10 represents the effect of the weight fractions of the lunar regolith simulant on the tensile mechanical properties of the specimens. The results show a significant decrease in tensile strength with the increase of the weight fractions, while interestingly the elastic

**Table 6** Mechanical properties of tensile specimens under different process parameters

No.	Weight fraction/wt.%	Printing temperature/°C	Printing speed/(mm·s <sup>-1</sup> )	$\sigma_b$ /MPa	$E$ /MPa
1	40	225	7	36.162	1674.18
2	50	225	7	23.055	1634.31
3	60	225	7	19.500	2443.41
4	40	230	7	22.580	1382.84
5	50	230	7	21.717	1702.24
6	60	230	7	20.556	1602.23
7	40	235	7	25.444	1531.78
8	50	235	7	23.041	1763.04
9	60	235	7	20.010	1803.54
10	40	225	8	32.392	1467.06
11	50	225	8	21.388	1682.22
12	60	225	8	18.818	1827.58
13	40	230	8	21.510	1322.97
14	50	230	8	19.428	1662.41
15	60	230	8	17.140	1594.13
16	40	235	8	24.752	1334.63
17	50	235	8	21.285	1455.93
18	60	235	8	17.389	1748.09
19	40	225	9	30.693	1152.13
20	50	225	9	18.215	1515.21
21	60	225	9	15.581	1443.74
22	40	230	9	20.898	1328.17
23	50	230	9	18.501	1460.74
24	60	230	9	15.424	1574.20
25	40	235	9	22.959	1271.04
26	50	235	9	18.319	1343.28
27	60	235	9	19.469	1763.33

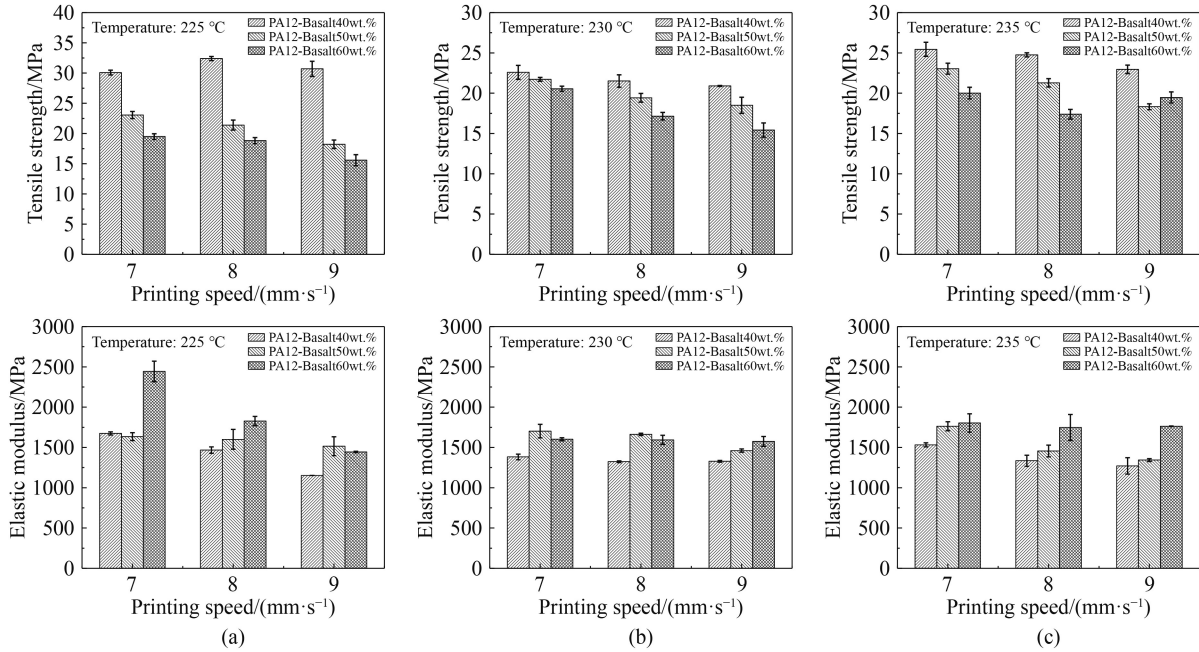


**Fig. 10** Effects of weight fraction on tensile mechanical properties with (a) 225 °C, (b) 230 °C, and (c) 235 °C.

modulus has the opposite behavior. This indicates that the lunar regolith simulant as a hard phase can significantly improve the deformation resistance of the structure, while the generation of cracks at the interface between PA12 and the lunar regolith simulant during the tensile process will reduce the tensile strength of the specimen. The relevant conclusions can be supported by the micromorphology of the specimens printed by the piston-based pellet extruder as shown in Fig. 9, which represents the horizontal and tangential plane micromorphology of the printed specimens parallel to the printing direction with different lunar regolith simulant weight fractions, respectively. The horizontal plane micromorphology shows that the lunar regolith simulant particles are uniformly distributed in the PA12 matrix material with an obvious interface profile. Meanwhile, the layers of the printed specimen are tightly bonded with only a small number of pore defects that can be observed from the tangential plane micromorphology, which is beneficial for the macroscopic mechanical properties of the structure.

### 3.3.2 Effects of printing temperature on tensile mechanical properties

From the economics of lunar habitat fabrication, the printing temperature is related to the energy consumption of the *in-situ* AM system. Meanwhile, it will also determine the rheological properties of the lunar regolith composite in the molten state, which will ultimately affect the mechanical properties of the printed specimens. Figure 11 represents the effect of printing temperature on

the tensile mechanical properties of the specimens. The results show that the printing temperature has varying effects on the tensile strength and elastic modulus of the printed specimens under different printing speed and weight fraction. When the weight fraction of the lunar regolith simulant up to 40 wt.%, the effect of temperature on the tensile strength is more significant. The variation of printing temperature will alter the viscosity and recrystallization process of the lunar regolith composite in the molten state, then affecting the melt extrusion process of the material and the mechanical properties of the printed structures. Hence, minimizing the energy consumption while maintaining the appropriate rheological properties of the molten lunar regolith composite will be very meaningful work for the *in-situ* fabrication of lunar regolith.

### 3.3.3 Effects of printing speed on tensile mechanical properties

The printing speed is related to the fabrication efficiency of the lunar habitat while affecting the mechanical properties of the printed structures. Figures 12 and 13 represent the stress–strain curves of the printed specimens after being placed for different periods at the printing temperature of 225 °C, respectively. The results show that the maximum tensile strength of the printed specimens reaches 36.2 MPa at 40 wt.% of the lunar regolith simulant and 7 mm/s of printing speed, which has obvious performance advantages compared with other works. The increase in printing speed can engender the issues of pore defects and weakened adhesion within the inter-filament and inter-layer, which results in a

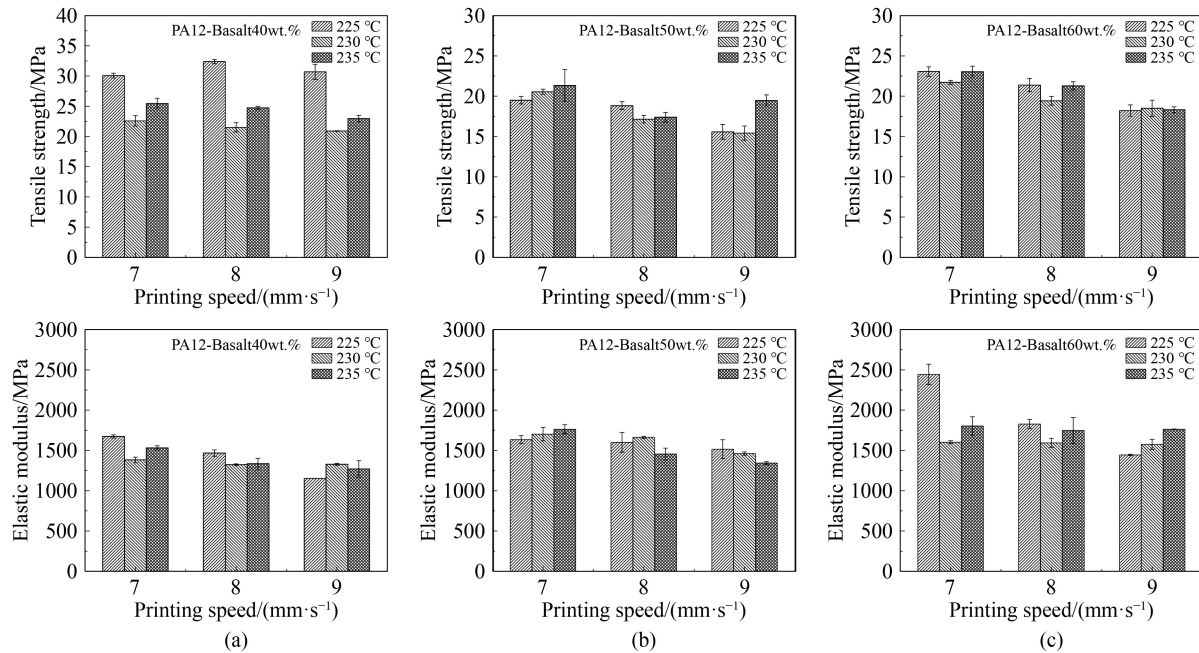


**Fig. 11** Effects of printing temperature on tensile mechanical properties with (a) PA12-Basalt40wt.%, (b) PA12-Basalt50wt.%, and (c) PA12-Basalt60wt.%.

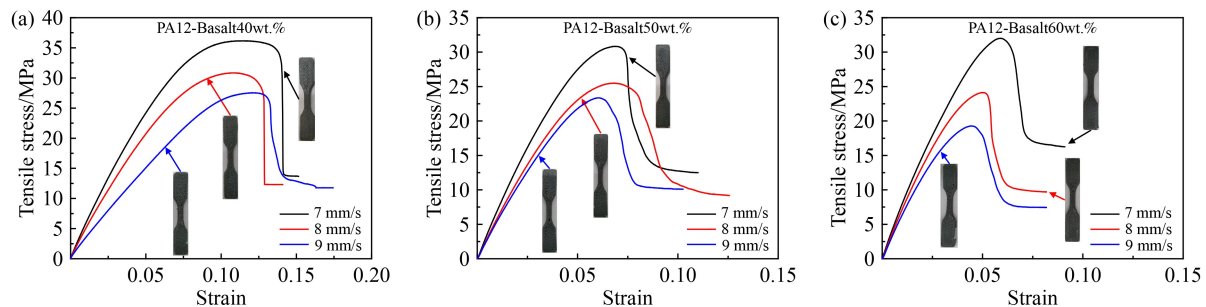


**Fig. 12** Stress-strain curves for the tensile specimens under different printing speed (3 days) with (a) PA12-Basalt40wt.%, (b) PA12-Basalt50wt.%, and (c) PA12-Basalt60wt.%.

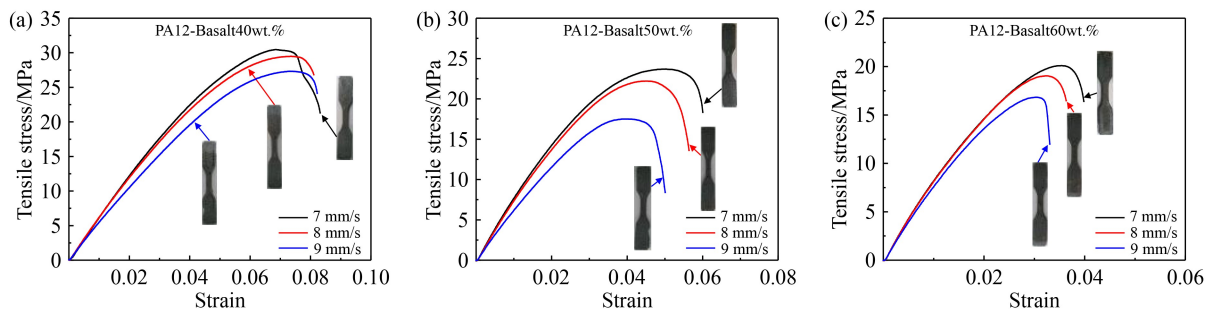


**Fig. 13** Stress-strain curves for the tensile specimens under different printing speed (30 days) with (a) PA12-Basalt40wt.%, (b) PA12-Basalt50wt.%, and (c) PA12-Basalt60wt.%.

significant decrease in the tensile strength of the printed specimens. Meanwhile, the phenomenon of material aging and performance degradation can be observed by comparing the stress-strain curves of the printed specimens for different placement periods, where the

stress decreases by 15%–30% and the strain decreases by 45%–66%. Therefore, it is necessary to consider the influence of process parameters on the mechanical properties of the printed structure and the material aging when performing the structural design.

### 3.3.4 Impact properties of lunar regolith composite specimens

The presence of numerous craters on the lunar surface is due to the moon frequently impacted by various meteorites. Therefore, the printed specimens of lunar regolith composites were subjected to impact tests, where Figs. 14(a) and 14(b) represent the absorbed energy and impact toughness of the printed specimens in the impact experiments, respectively. The results show that the increase in weight fraction of the lunar regolith simulant significantly results in the enhancement of the absorbed energy and impact toughness of the printed specimens, which is mainly due to the lunar regolith simulant that uniformly distributed in the PA12 matrix material as a hard phase can absorb more impact energy during the fracture process. Meanwhile, the influence of printing direction on the impact resistance of printed specimens is

also not negligible, and the effect of the printing direction is more significant with the increase of weight fraction.

### 3.4 Manufacturing verification via screw-based pellet extruder

The feasibility and excellent mechanical properties of 3D printing lunar regolith-based composites were verified using a piston-based pellet extruder. To further improve the utilization of lunar regolith materials, the performance of printed structures, and to be suitable for printing large-scale components in the harsh environment of the moon, an efficient robot-assisted screw-based pellet extruder was developed. Figures 15(a) and 15(b) represent the schematic platform and physical platform of the screw-based pellet extruder, respectively. The screw-based pellet extruder mounted on a multi-axis robot provides the feasibility to achieve the printing of large-scale or

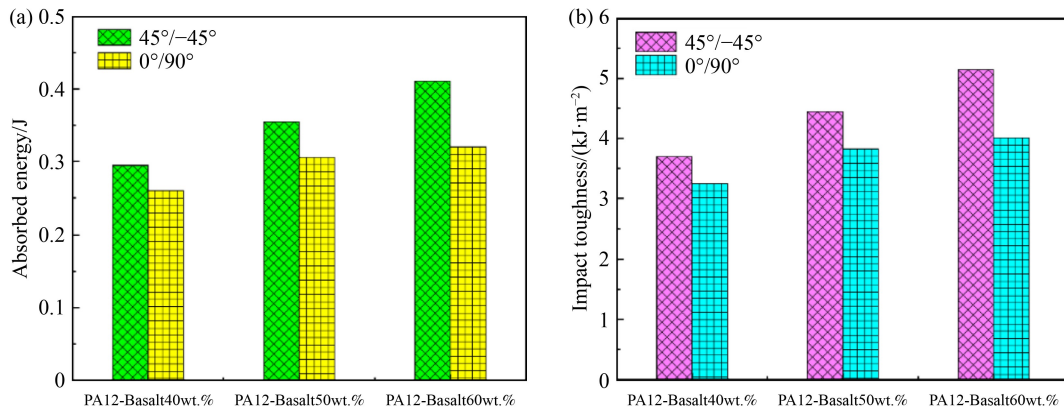


**Fig. 14** Impact testing results of lunar regolith composite at different basalt weight fractions: (a) absorbed energy and (b) impact toughness.

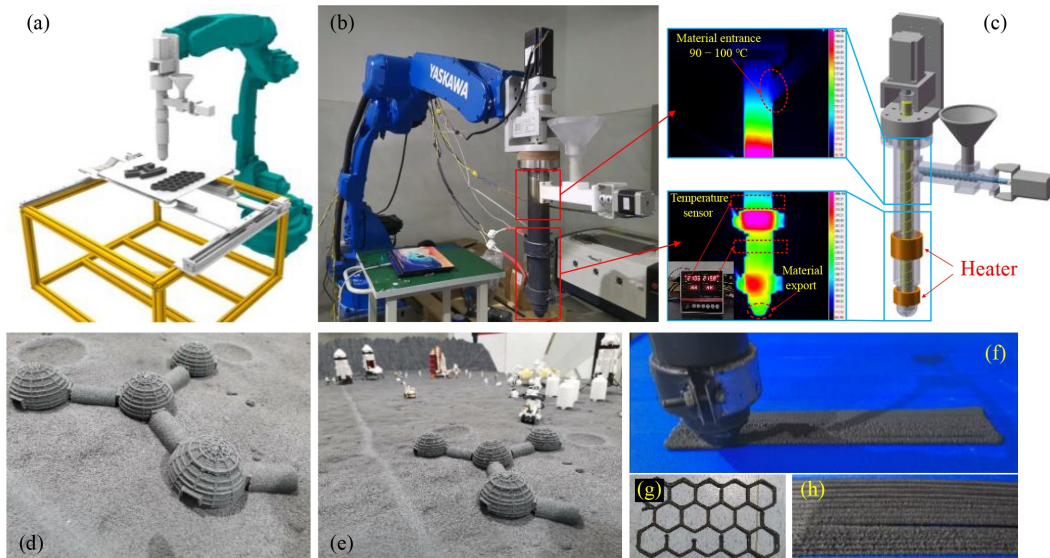


**Fig. 15** Platform of screw-based pellet extruder: (a) schematic platform, (b) physical platform, (c) infrared image of the heated nozzle, (d, e) printed lunar habitat model, (f) printing process, (g) printed honeycomb structure, and (h) printed board structure.

complex curved components. The variable diameter extrusion screw inside the extruder not only has excellent adaptability to the lunar regolith materials with a wide particle size distribution and irregular shape but also the shearing force of the extrusion screw allows for more uniform mixing of the lunar regolith with the molten polymer material. Meanwhile, a stable extrusion force can be provided by the extrusion motor to ensure the continuity of the extruded molten material and improve the performance of the printed structure. Based on the geometrical parameters of the extrusion screw and feeding screw, the motor speed can be regulated to implement the matching of the conveying and extrusion volumes of the lunar-based composite material, thereby ensuring the continuous and smooth extrusion of the molten material. The infrared image of the heated nozzle is shown in Fig. 15(c). The independent temperature-controlled multi-segment heaters installed outside the extruder can be used to achieve gradient control of the nozzle temperature, which assures adequate melting and homogeneous extrusion of lunar regolith-based composite material. Figures 15(f)–15(h) show the process and components for printing lunar regolith-based composites utilizing the screw-based high-pressure pellet extruder. Table 7 represents the process parameters of the extruder. It can be concluded that the weight fraction of the lunar regolith simulant can reach up to 80 wt.%, which indicates the apparent advantage in improving the lunar regolith utilization. Furthermore, the feasibility of using the high-pressure 3D printing system to complete the printing of complex structures is verified by the printed lunar habitat model as shown in Figs. 15(d) and 15(e).

**Table 7** Process parameters of screw-based pellet extrusion

Parameter	Value
Basalt weight fraction	80 wt. %
Layer height	4 mm
Nozzle diameter	5 mm
Raster gap	4 mm
Printing temperature	235 °C
Bed temperature	70 °C
Extrusion screw rotation speed	8–10 r/min
Feeding screw rotation speed	12.5–15 r/min
Robot motion speed	8–9 mm/s
Infill percentage	100%

## 4 Conclusions

In this work, lunar regolith-based composites are blended with high-performance thermoplastic polymers by a high-pressure melt extrusion molding at relatively low temperatures. It provides an effective approach compared with direct melt lunar regolith mixtures to minimize energy and time consumption and ensure the mechanical

properties of printed structures. The thermal properties, micromorphology, and flowability of the feeding material were assessed to quantify the physical parameters of the powder material and determine the printing process window. The effects of the weight fraction, printing speed, and printing temperature on the mechanical properties were quantitatively investigated. The maximum tensile strength and impact strength reach 36.2 MPa and 5.15 kJ/m<sup>2</sup> respectively, which show significant improvement as compared with previously reported works. The feasibility and optimal process window of the melt extrusion molding process for 3D printing of lunar regolith-based composites were preliminarily verified. The screw-based high-pressure pellet extruder enables to improve the weight fraction of lunar regolith up to 80 wt.%. The lunar regolith-based composites via screw-based extrusion molding can fully utilize the *in-situ* source on lunar.

## Nomenclature

### Abbreviations

AM	Additive manufacturing
DSC	Differential scanning calorimetry
ISRU	<i>In-situ</i> resource utilization
MAM	Motor-assisted microsyringe
SEM	Scanning electron microscope
TGA	Thermogravimetric analysis

### Variables

$a_k$	Impact toughness
$A_k$	Impact energy
$E$	Young's modulus
$T_m$	Melting peak temperature
$T_r$	Recrystallization peak temperature
$\sigma_b$	Tensile strength

**Acknowledgements** This work was supported by the National Key R&D Program of China (Grant No. 2017YFB1102800), the National Natural Science Foundation of China for Excellent Young Scholars (Grant No. 11722219), the National Natural Science Foundation of China (Grant No. 51905439), and the Emerging (Interdisciplinary) Cultivation Project of Northwestern Polytechnical University, China (Grant Nos. 19SH030403, 20SH030201, and 21SH030601).

**Conflict of Interest** The authors declare that they have no conflict of interest.

## References

1. Wu W R, Yu D Y. Development of deep space exploration and its

- future key technologies. *Journal of Deep Space Exploration*, 2014, 1(1): 5–17 (in Chinese)
2. Wu W R, Liu J Z, Tang Y H, Yu D Y, Yu G B, Zhang Z. China lunar exploration program. *Journal of Deep Space Exploration*, 2019, 6(5): 405–416 (in Chinese)
  3. Matsumoto K, Kamimori N, Takizawa Y, Kato M, Oda M, Wakabayashi S, Kawamoto S, Okada T, Iwata T, Ohtake M. Japanese lunar exploration long-term plan. *Acta Astronautica*, 2006, 59(1–5): 68–76
  4. Braun M, Gollins N, Trivino V, Hosseini S, Schonenborg R, Landgraf M. Human lunar return: an analysis of human lunar exploration scenarios within the upcoming decade. *Acta Astronautica*, 2020, 177: 737–748
  5. Benaroya H, Bernold L. Engineering of lunar bases. *Acta Astronautica*, 2008, 62(4–5): 277–299
  6. Marov M Y, Slyuta E N. Early steps toward the lunar base deployment: some prospects. *Acta Astronautica*, 2021, 181: 28–39
  7. Sanders G B, Larson W E. Integration of *in-situ* resource utilization into lunar/mars exploration through field analogs. *Advances in Space Research*, 2011, 47(1): 20–29
  8. Sanders G B, Larson W E. Progress made in lunar *in-situ* resource utilization under NASA's exploration technology and development program. *Journal of Aerospace Engineering*, 2013, 26(1): 5–17
  9. Meurisse A, Carpenter J. Past, present and future rationale for space resource utilisation. *Planetary and Space Science*, 2020, 182: 104853
  10. Rasera J N, Cilliers J J, Lamamy J A, Hadler K. The beneficiation of lunar regolith for space resource utilisation: a review. *Planetary and Space Science*, 2020, 186: 104879
  11. Zhang T, Chao C Y, Yao Z X, Xu K, Zhang W X, Ding X L, Liu S T, Zhao Z, An Y H, Wang B, Yu S F, Wang B, Chen H W. The technology of lunar regolith environment construction on earth. *Acta Astronautica*, 2021, 178: 216–232
  12. Shkuratov Y G, Bondarenko N V. Regolith layer thickness mapping of the moon by radar and optical data. *Icarus*, 2001, 149(2): 329–338
  13. Miller J, Taylor L, Zeitlin C, Heilbronn L, Guetersloh S, DiGiuseppe M, Iwata Y, Murakami T. Lunar soil as shielding against space radiation. *Radiation Measurements*, 2009, 44(2): 163–167
  14. Li C L, Hu H, Yang M F, Pei Z Y, Zhou Q, Ren X, Liu B, Liu D W, Zeng X G, Zhang G L, Zhang H B, Liu J J, Wang Q, Deng X J, Xiao C J, Yao Y G, Xue D S, Zuo W, Su Y, Wen W B, Ouyang Z Y. Characteristics of the lunar samples returned by Chang'e-5 mission. *National Science Review*, 2022, 9(2): nwab188
  15. Zhang H, Zhang X, Zhang G, Dong K Q, Deng X J, Gao X S, Yang Y D, Xiao Y, Bai X, Liang K X, Liu Y W, Ma W B, Zhao S F, Zhang C, Zhang X J, Song J, Yao W, Chen H, Wang W H, Zou Z G, Yang M F. Size, morphology, and composition of lunar samples returned by Chang'e-5 mission. *Science China Physics, Mechanics & Astronomy*, 2021, 65(2): 229511
  16. Hu S, He H C, Ji J L, Lin Y T, Hui H J, Anand M, Tartèse R, Yan Y H, Hao J L, Gu L X, Guo Q, He H Y, Ouyang Z Y. A dry lunar mantle reservoir for young mare basalts of Chang'e-5. *Nature*, 2021, 600(7887): 49–53
  17. Tian H C, Wang H, Chen Y, Yang W, Zhou Q, Zhang C, Lin H L, Huang C, Wu S T, Jia L H, Xu L, Zhang D, Li X G, Chang R, Yang Y H, Xie L W, Zhang D P, Zhang G L, Yang S H, Wu F Y. Non-KREEP origin for Chang'e-5 basalts in the Procellarum KREEP Terrane. *Nature*, 2021, 600(7887): 59–63
  18. Li Q L, Zhou Q, Liu Y, Xiao Z Y, Lin Y T, Li J H, Ma H X, Tang G Q, Guo S, Tang X, Yuan J Y, Li J, Wu F Y, Ouyang Z Y, Li C L, Li X H. Two-billion-year-old volcanism on the moon from Chang'e-5 basalts. *Nature*, 2021, 600(7887): 54–58
  19. Costes N C, Carrier W D, Mitchell J K, Scott R F. Apollo 11 soil mechanics investigation. *Science*, 1970, 167(3918): 739–741
  20. Sibille L, Carpenter P K, Schlagheck R A, French R A. Lunar Regolith Simulant Materials: Recommendations for Standardization, Production, and Usage. NASA Technical Reports NASA/TP-2006-214605, 2006
  21. Zheng Y C, Wang S J, Ouyang Z Y, Zou Y L, Liu J Z, Li C L, Li X Y, Feng J M. CAS-1 lunar soil simulant. *Advances in Space Research*, 2009, 43(3): 448–454
  22. Alshibli K A, Hasan A. Strength properties of JSC-1A lunar regolith simulant. *Journal of Geotechnical and Geoenvironmental Engineering*, 2009, 135(5): 673–679
  23. Arslan H, Sture S, Batiste S. Experimental simulation of tensile behavior of lunar soil simulant JSC-1. *Materials Science and Engineering: A*, 2008, 478(1–2): 201–207
  24. Kalapodis N, Kampas G, Ktenidou O J. A review towards the design of extraterrestrial structures: from regolith to human outposts. *Acta Astronautica*, 2020, 175: 540–569
  25. Isachenkov M, Chugunov S, Akhatov I, Shishkovsky I. Regolith-based additive manufacturing for sustainable development of lunar infrastructure—an overview. *Acta Astronautica*, 2021, 180: 650–678
  26. Khoshnevis B, Bodiford M P, Burks K H, Ethridge E, Tucker D, Kim W, Toutanji H, Fiske M R. Lunar contour crafting—a novel technique for ISRU-based habitat development. In: *Proceedings of the 43rd AIAA Aerospace Science Meeting and Exhibit*. Reno: AIAA, 2005, AIAA 2005-538
  27. Davis G, Montes C, Eklund S. Preparation of lunar regolith based geopolymer cement under heat and vacuum. *Advances in Space Research*, 2017, 59(7): 1872–1885
  28. Wang K T, Lemougna P N, Tang Q, Li W, Cui X M. Lunar regolith can allow the synthesis of cement materials with near-zero water consumption. *Gondwana Research*, 2017, 44: 1–6
  29. Toutanji H A, Evans S, Grugel R N. Performance of lunar sulfur concrete in lunar environments. *Construction & Building Materials*, 2012, 29: 444–448
  30. Zhou S Q, Zhu X Y, Lu C H, Li F. Synthesis and characterization of geopolymer from lunar regolith simulant based on natural volcanic scoria. *Chinese Journal of Aeronautics*, 2022, 35(1): 144–159
  31. Cesaretti G, Dini E, De Kestelier X, Colla V, Pambaguian L. Building components for an outpost on the lunar soil by means of a novel 3D printing technology. *Acta Astronautica*, 2014, 93: 430–450
  32. Krishna Balla V, Roberson L B, O'Connor G W, Trigwell S, Bose S, Bandyopadhyay A. First demonstration on direct laser fabrication of lunar regolith parts. *Rapid Prototyping Journal*, 2012, 18(6): 451–457

33. Zhao H, Meng L, Li S Y, Zhu J H, Yuan S Q, Zhang W H. Development of lunar regolith composite and structure via laser-assisted sintering. *Frontiers of Mechanical Engineering*, 2022, 17(1): 6
34. Meurisse A, Makaya A, Willsch C, Sperl M. Solar 3D printing of lunar regolith. *Acta Astronautica*, 2018, 152: 800–810
35. Goulas A, Friel R J. 3D printing with moondust. *Rapid Prototyping Journal*, 2016, 22(6): 864–870
36. Goulas A, Harris R A, Friel R J. Additive manufacturing of physical assets by using ceramic multicomponent extra-terrestrial materials. *Additive Manufacturing*, 2016, 10: 36–42
37. Goulas A, Binner J G P, Harris R A, Friel R J. Assessing extraterrestrial regolith material simulants for *in-situ* resource utilisation based 3D printing. *Applied Materials Today*, 2017, 6: 54–61
38. Fateri M, Gebhardt A. Process parameters development of selective laser melting of lunar regolith for on-site manufacturing applications. *International Journal of Applied Ceramic Technology*, 2015, 12(1): 46–52
39. Liu M, Tang W Z, Duan W Y, Li S, Dou R, Wang G, Liu B S, Wang L. Digital light processing of lunar regolith structures with high mechanical properties. *Ceramics International*, 2019, 45(5): 5829–5836
40. Jakus A E, Koube K D, Geisendorfer N R, Shah R N. Robust and elastic lunar and martian structures from 3D-printed regolith inks. *Scientific Reports*, 2017, 7(1): 44931
41. Liu J X, Cui Y, Yang J P, Wu Z S. Effect of basalt composition and mineral on high temperature melting process. *Journal of Yanshan University*, 2017, 41(4): 323–328 (in Chinese)